Journal of the European Ceramic Society 18 (1998) 2351–2364

PII: S0955-2219(98)00242-8
0955-2219/99/$—see front matter

Mullite Based Oxidation Protection for SiC–C/C Composites in Air at Temperatures Up to 1900 K

H. Fritze,[a]* J. Jojic,[a] T. Witke,[b] C. Rüscher,[c] S. Weber,[d] S. Scherrer,[d] R. Weiß,[e] B. Schultrich[b] and G. Borchardt[a]

[a]Institut für Allgemeine Metallurgie and SFB 180, Technische Universität Clausthal, Robert-Koch-Straße 42, D-38678 Clausthal-Zellerfeld, Germany
[b]Fraunhofer-Institut für Werkstoffphysik und Strahltechnologie Winterbergstraße 28, D-01277 Dresden, Germany
[c]Institut für Mineralogie, Universität Hannover, Welfengarten 1, D-30167 Hannover, Germany
[d]Laboratoire de Métallurgie Physique et Sciences des Matériaux, Ecole des Mines de Nancy, Parc de Saurupt, F-54042 Nancy Cedex, France
[e]Schunk Kohienstofftechnik GmbH, D-35339 Gießen, Germany

Abstract

For an industrial Si–SiC coated C/C material (reference material) the temperature dependence of the linear rate of mass loss is interpreted in the temperature range 773 < T < 1973 K. The Arrhenius plot of the thermogravimetrically determined oxidation rate shows four typical regimes. Only in the temperature range 1323 < T < 1823 K is the oxidation rate close to or lower than the limit for long-term application. Pulsed Laser Deposition (PLD) allows the ablation of nonconductive and high melting targets and the preparation of films with complex composition. High energy impact CO_2 laser pulses ($j = 3{\cdot}10^7$ W cm^{-2}) lead to melting and evaporation of the target material in a single step. Therefore the flux of the metal components is stoichiometric. Deposited green layers did not show IR peaks typical for mullite. After a short oxidation treatment (15 min at 1673 K) the formation of mullite in the coating was completed as was confirmed by IR spectroscopy and XRD investigations. Thin PLD-mullite layers (900 nm) did not markedly improve the oxidation resistance of the reference material in the high temperature range 1473 < T < 1973 K. However, a preoxidation treatment of the substrate material and mullite coatings with a thickness of 2·5 μm improved the oxidation behaviour significantly. Because of SiO_2 formation at the mullite–SiC interface all samples exhibited a mass increase on oxidation. The inward diffusion of oxygen across the outer mullite-containing layer controlled the kinetics of the reaction as was deduced from ^{18}O diffusivity measurements in PLD mullite layers. The calculated oxidation rates resulting from the diffusion parameters in SiO_2 and mullite are close to the thermogravimetric data. For oxidation durations of three days only amorphous SiO_2 is formed at the mullite–SiC interface. © *1999 Elsevier Science Limited. All rights reserved*

1 Introduction

Because of their excellent mechanical properties at high temperatures, carbon/carbon composites (C/C) are very attractive for structural applications. Without oxidation protection, however, carbon materials do not withstand oxidising atmospheres.[1–3]

Depending on the duration of application, the acceptable carbon loss determines the maximum oxidation rate which can be tolerated. As suggested by K. L. Luthra,[4] a reduction in the wall thickness of a typical structural component of 0·3 mm within 2000 h (long term application) is considered acceptable. This criterion results in a maximum mass loss rate of $3{\cdot}10^{-2}$ mg cm^{-2} h^{-1} corresponding to an operation temperature limit of 723 K for unprotected C/C materials in air.[4] Depending on the degree of internal oxidation, the tolerable mass loss rate could be much lower than the rate mentioned

*To whom correspondence should be addressed. e-mail: hfritze@mit.edu

above. In order to improve the oxidation resistance at higher temperatures suitable oxygen diffusion barriers have to be developed.

Mullite ceramics (3 Al_2O_3·2 SiO_2) are promising candidate materials for high temperature applications. Mullite coated SiC exhibits excellent oxidation resistance in dry air by forming a slowly growing SiO_2 scale at the mullite–SiC interface.[5] Depending on the SiO_2 content mullite forms a liquid phase which can close cracks and pores. For example, a freshly prepared plasma-sprayed mullite coating gave SiC substrates excellent protection under thermal cycling conditions.[6]

In this investigation effort was focused on the effect of protective outer mullite layers produced by Pulsed Laser Deposition (PLD). Based on experimental data the oxidation behaviour in the high temperature range ($1473 < T < 1973$ K) in air is discussed. Additionally, diffusion coefficients of ^{18}O in PLD mullite layers are presented.

2 Sample Preparation

The starting materials were thin two-dimensional C/C slabs ($2\times20\times20\,mm^3$) infiltrated with liquid silicon under pressure and coated with SiC by CVD (C/C–Si–SiC, Schunk Kohlenstofftechnik, Germany). This commercial material is used as the reference material in this study. Prior to the mullite deposition the samples were preoxidized in air (4 h, 1673 K). The resulting SiO_2 layer of about $0{\cdot}2\,\mu m$ serves as a bond coat. Subsequently, mullite was deposited by Pulsed Laser Deposition (PLD). High energy impact CO_2 laser pulses ($\lambda = 10{\cdot}6\,\mu m$, $\Delta t = 170\,\mu s, j = 3{\cdot}10^7\ W\,cm^{-2}$) led to melting and evaporation of the target material in a single step. The flux of the metal components was stoichiometric. As the work was carried out under reduced pressure ($p_{tot} = 10^{-3}$ Pa) the oxygen content of the PLD layer decreased.[7]

For these targets (sintered mullite powder, Baikowski Chimie, France) the typical deposition rate was $100\,nm\,s^{-1}$. Even with target rotation deposition rates up to $500\,nm\,s^{-1}$ can be reached only by using larger targets. The substrate temperature did not rise to more than 373 K.

Figure 1 shows schematically the coating steps and the corresponding layer thicknesses.

IR-reflection spectra between 650 and $1300\,cm^{-1}$ of the target material and of PLD coatings on SiC heated at 1673 K for 15 min are shown in Fig. 2. Both spectra show similar band shapes with a peak at about $720\,cm^{-1}$ and broad structures between 800 and $1000\,cm^{-1}$ and between 1050 and $1200\,cm^{-1}$. Therefore, the IR reflection spectra indicate that mullite is formed after only a short oxidation.

The formation of mullite was also confirmed by XRD investigations.

3 Microstructure of the Reference Material

On the surfaces of the reference material (C/C–Si–SiC) a two-dimensional network of cracks with an average spacing of $d_s = 0{\cdot}4$ mm (Figs 3 and 4) was observed. Because of thermal expansion coefficient mismatch between C/C (parallel to the fibres: $\alpha_{C/C\|} = 0{\cdot}8{\cdot}10^{-6}\ K^{-1}$) and SiC ($\alpha_{sic} = 6{\cdot}1{\cdot}10^{-6}\ K^{-1}$) this network structure will exist after cooling down from the CVD processing temperature. The cracks extend to the C/C surface with an average width $\bar{d}_w = 2\,\mu m$ at room temperature.

The width of one crack can be described by:

$$\begin{aligned} d_W(T) &= \left(\alpha_{C/C} - \alpha_{sic}\right)(T - T_C)d_s \quad \text{for} \quad T < T_C \\ d_W(T) &= 0 \qquad\qquad\qquad\qquad\quad \text{for} \quad T \geq T_C \end{aligned}$$

The crack width of $d_W = 2\,\mu m$ at room temperature leads to a crack closing temperature $T_C = 1243$ K which corresponds to the lower limit of the CVD processing.

Assuming a uniform distribution of the crack width in the range from $d_{W0}(T)$ to $d_{W1}(T)$ the average crack width $\bar{d}_W(T)$ results from

$$\bar{d}_W(T) = \frac{d_{W0}(T) + d_{W1}(T)}{2} \qquad (2)$$

if all cracks are open ($d_{W0}(T) > 0$). With increasing temperature the narrowest cracks start to close ($d_{W0}(T) = 0$) and the average crack width can be described by:

Table 1. PLD: Transfer of composition

Sample	*Treatment*	*Composition [at.%]*				$c_A/(c_{A1} + c_{Si})$
		c_c	c_o	c_{A1}	c_{Si}	
Mullite target[a]	Sintered powder	–	61·9	28·6	9·5	0·752
Mullite layer[b]	Green layer	2·2	52·1	34·4	11·3	0·753

[a]Calculated from nominal powder composition.
[b]WDX analysis, $E_{prim} = 6$ KeV.

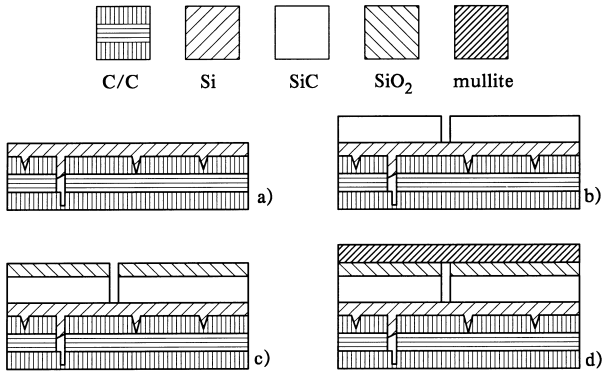

Fig. 1. Coating steps and layer thicknesses. (a) Si infiltrated C/C material, (b) +50 μm SiC (CVD), (c) +0.2 μm SiO_2 (pre-oxidation), (d) +2·5 μm mullite (PLD).

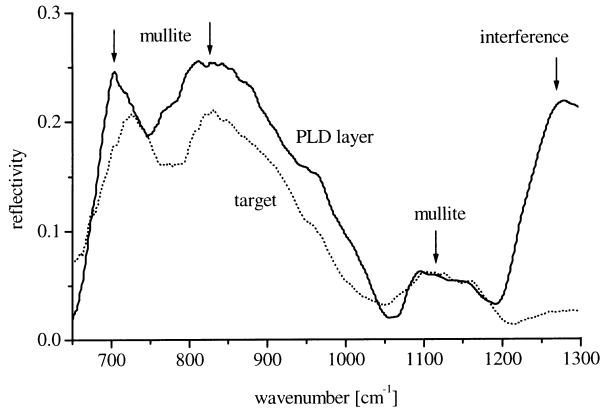

Fig. 2. Reflectivity of the target in comparison with the reflectivity of a PLD coating on SiC annealed in air at 1673 K for 15 min.

$$\bar{d}_W(T) = \frac{1}{2}\frac{d_{W1}(T)^2}{d_{W1}(T) - d^*_{W0}(T)} \tag{3}$$

With:

$$d^*_{W0}(T) = (\alpha_{C/C} - \alpha_{SiC})(T - T_{C0})d_s \tag{4}$$

T_{C0} corresponds to the closing temperature of the cracks of width d_{W0}.

In case of a square network with spacing d_s the fractional area of the cracks f_R would be given by:

$$f_R = \frac{2\bar{d}_W}{d_S} \tag{5}$$

4 Oxidation Behaviour of the Reference Material (C/C–Si–SiC)

4.1 Isothermal oxidation in air

The weight change of the specimens was measured as a function of time using an automatic thermobalance. The thermogravimetric experiments were started by lowering the sample into the hot reaction gas (ambient air). The reaction tube and the sample

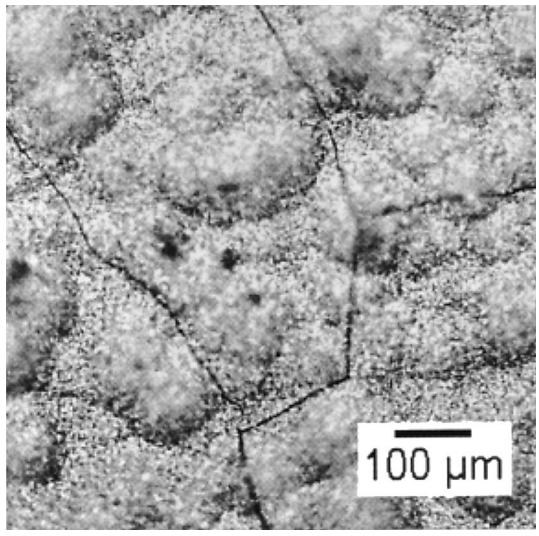

Fig. 3. Microstructure of the Si–SiC coated C/C material (surface).

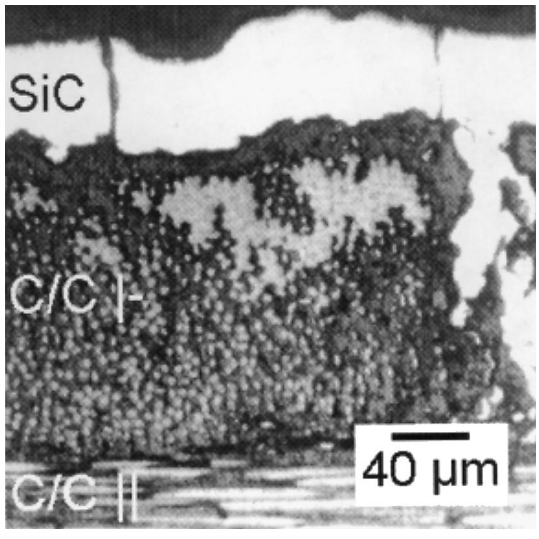

Fig. 4. Microstructure of the Si–SiC coated C/C material (cross-section).

support were made from alumina and were baked out over a prolonged period of time prior to the experiments. Independent of the porosity of the samples the mass change Δm was related to the geometrical surface area A_0 of the samples.

The samples exhibited a mass loss in the whole temperature range as shown in Figs 5 and 6 which led to fibre bum out at the bottom of the cracks (Fig. 7).

For times which are interesting for technical applications the mass loss can be expressed as a linear function of time t:

$$\frac{\Delta m(t)}{A_0} = k_L \Delta t \tag{6}$$

The resulting Arrhenius plot of the oxidation rate is discussed in detail in section 4.4.

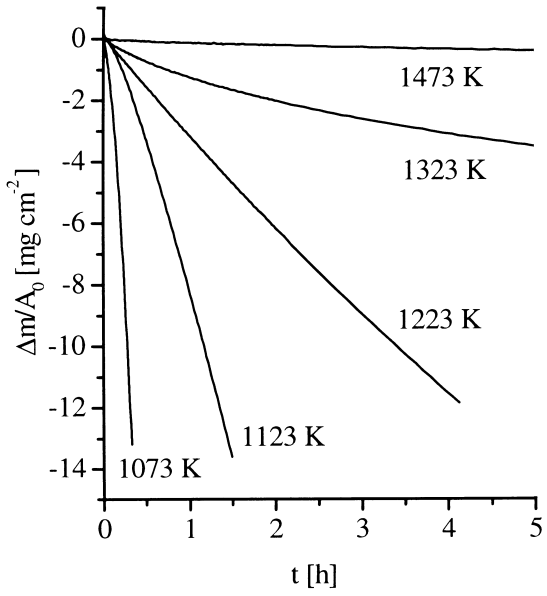

Fig. 5. Specific mass loss of the reference material (C/C–Si–SiC) in the low temperature range.

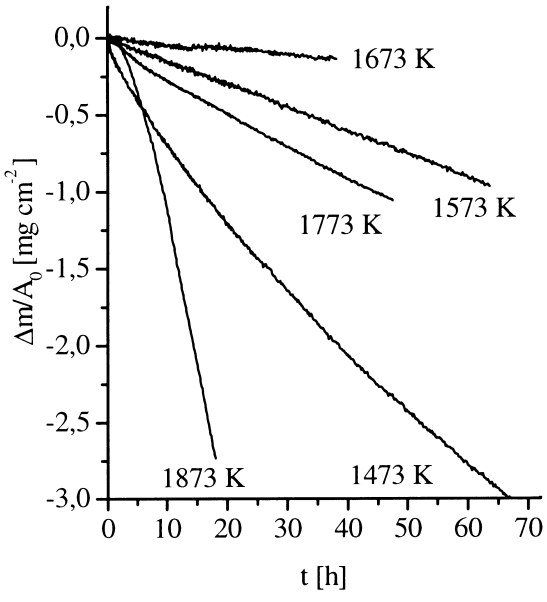

Fig. 6. Specific mass loss of the reference material (C/C–Si–SiC) in the high temperature range.

4.2 Phase identification

The oxidation treatments lead to the formation of SiO_2. This process is not observable by TGA because of the dominance of carbon burn out.

Infrared measurements are useful because SiO_2 shows characteristic lattice bands in the mid infrared spectral range.

Figure 8 shows reflection spectra of the reference material after the TGA measurements. The oxidation for 40 h at 1673 K led to a broad structure between 1060 and 1240 cm^{-1} typically obtained for amorphous SiO_2. With increasing temperature a splitting of this peak is observable which indicates the crystallization of SiO_2.[8] The phase transformation

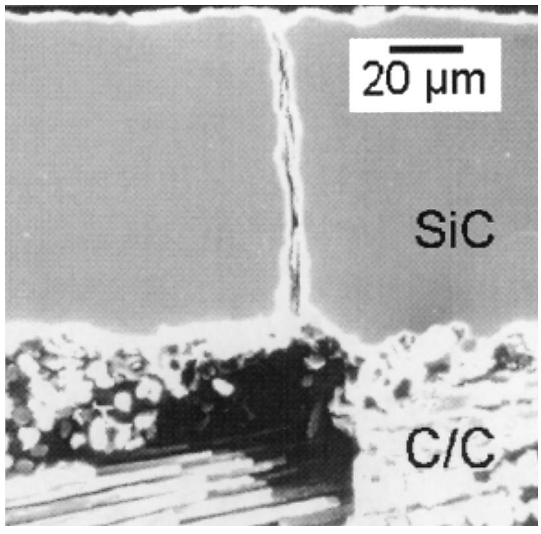

Fig. 7. Carbon burn out at the bottom of the cracks (C/C–Si–SiC).

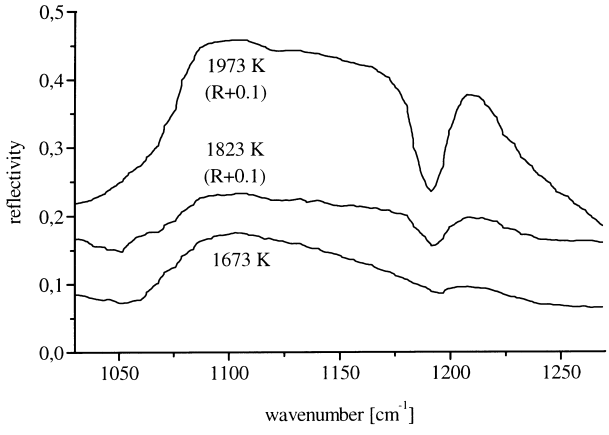

Fig. 8. Reflectivity of the oxidized reference material (in parenthesis: shift of the curves in the diagram).

causes a volume contraction[9] and the protectiveness of the SiO_2 layers is reduced.

4.3 Rate limiting steps

The measured temperature dependence of the reaction rate allows the determination of the rate limiting step. Additionally, the calculation of the virtual reaction rate (consideration of isolated reactions steps) is necessary if several steps exhibit the same temperature dependence. In the case of mixed control the overall reaction rate k for a two-step process can be expressed via the individual reaction rate constants k_1 and k_2:

$$\frac{1}{k} = \frac{1}{k_1} + \frac{1}{k_2} \tag{7}$$

Carbon rapidly reacts with oxygen, forming gaseous carbon oxides CO_2 and CO:

$$C + O_2 \rightleftharpoons CO_2(g) \tag{8}$$

$$C + \frac{1}{2}O_2 \rightleftharpoons CO(g) \tag{9}$$

Both reactions cause mass loss. Because of the standard free energy values the formation of CO is predominant above 973 K. Reaction (9) implies the relation

$$-2j_{O_2} = j_{CO} \tag{10}$$

from which follow a convectional outward gas flow j_G and the corresponding velocity v:

$$j_G \approx j_{CO} + j_{O_2} = -j_{O_2} \tag{11}$$

$$v = \frac{j_{O_2}}{n_G} \tag{12}$$

n_G is the total gas density. In ambient air, above 1273 K significant passive oxidation of SiC is expected.

$$SiC + \frac{3}{2}O_2 \rightleftharpoons SiO_2(s) + CO(g) \tag{13}$$

$$SiC + O_2 \rightleftharpoons SiO(g) + CO(g) \tag{14}$$

Reaction (13) results in a mass gain. It should be noted that a convectional inward flow occurs. The formation of SiO [active oxidation, reaction (14)] can occur only locally in regions with sufficiently low oxygen partial pressure.[3]

Following eqn (9) the factor $-24u$ (u = atomic mass unit) gives the conversion from oxygen flux density j_{O2} to mass change (i.e. 2 moles of carbon lost for each mole of oxygen consumed):

$$\frac{1}{A_0}\frac{\Delta m}{\Delta t} = -24u j_{O_2} f \tag{15}$$

The fractional area of oxygen transport f depends on the rate determing step.

With protective films on the surface, the oxidation of the coated C/C samples involves the following processes (illustrated in Fig. 9). The fractional area f of the oxygen transport/reaction zone is given in parenthesis:

1. O_2 inward diffusion across the gas boundary layer ($f = 1$). The flux can be expressed by Fick's first law. The term vn_{O2} takes into account a convectional flux:

$$j_{O_2} = -D_G \frac{\partial n_{O_2}}{\partial x} + v n_{O_2} \tag{16}$$

Here, n_{O_2} is the concentration of O_2 across the boundary layer, x is the distance from the surface. For the gas interdiffusion coefficient the expression given by Geiger and Poirier[10] was used:

$$D_G = D_{G0}\frac{T^{1.75}}{P} \tag{17}$$

D_{G0} depends on the details of the multicomponent transport in the boundary layer, p is the total pressure.

2. O_2 diffusion through cracks and pores ($f = f_R$). The flux can be expressed by Fick's first law, too:

$$j_{O_2} = -\bar{D}\frac{\partial n_{O_2}}{\partial x} + v n_{O_2} \tag{18}$$

Here, x is the distance from the bottom of the cracks. $\bar{D}(D_G, D_K)$ describes a modified gas diffusion coefficient for small crack dimensions. If the mean free path of the gas molecules is of the same order as the crack width d_W, gas transport occurs by Knudsen diffusion. For crack widths smaller than about 10 nm Knudsen diffusion will be important at $p = 10^5$ Pa and $T = 1673$ K which can be estimated by using the expression for cylindrical pores:

$$D_K = \frac{1}{3}\sqrt{\frac{8RT}{\pi M}}d \tag{19}$$

3. Solid state diffusion through the coating ($f = 1 - f_R \approx 1$). The flux of oxygen atoms can be expressed by:

$$j_o = D_s \frac{\Delta n_o}{d_L} \tag{20}$$

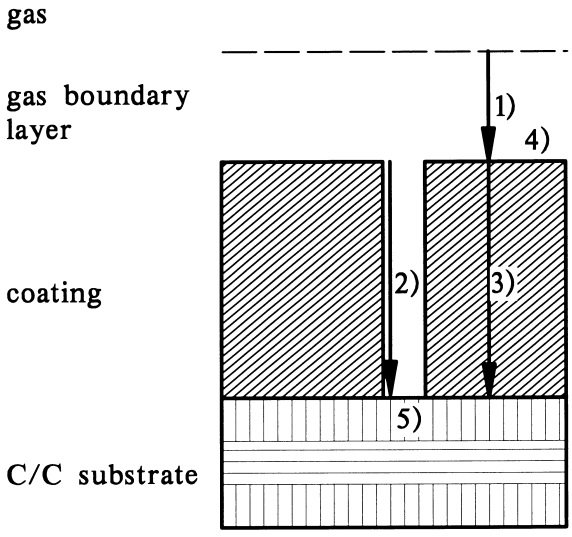

Fig. 9. Possible rate limiting steps during oxidation of coated C/C material (see text).

Δn is the concentration drop of oxygen across the coating with a thickness d_L. In case of solid state diffusion an exponential temperature dependence of the diffusivity is valid:

$$D_B = D_{B0} e^{\frac{-E_B}{RT}} \tag{21}$$

4. Reaction at the gas-coating interface ($f = 1$). The reaction rate can be expressed as:

$$j_{o_2} = k_I e^{-\frac{E_I}{RT}} \tag{22}$$

k_I and E_I are the preexponential factor and the activation energy, respectively.

5. Reaction at the gas–C/C interface (porous substrates: $f \geq 1$). The reaction rate can be expressed as:

$$j_{o_2} = k_c e^{-\frac{E_c}{RT}} \tag{23}$$

6. Outward diffusion of gaseous reaction products analogous to the diffusion steps 1, 2 and 3.

4.4 Analysis of the reaction kinetics

The Arrhenius plot of the oxidation rate (Fig. 10) shows typical regimes which are in the following:

I. Exponential temperature dependence ($T < 1123$ K). The reaction rate is determined by the reaction at the gas–C/C interface. The activation energy for the C/C–Si–SiC material ($E_c = 142$ kJ mol^{-1}, curve A in Fig. 10) and for the uncoated C/C material ($\tilde{E}_c = 150$ kJ mol^{-1}, curve B in Fig. 10) are similar. This correspondence indicates that the same mechanism determines the reaction rate in both cases. In this temperature range the crack width in the CVD layer is very large and does not influence the reaction rate. Solid state diffusion can be neglected because of the value of the activation energy.

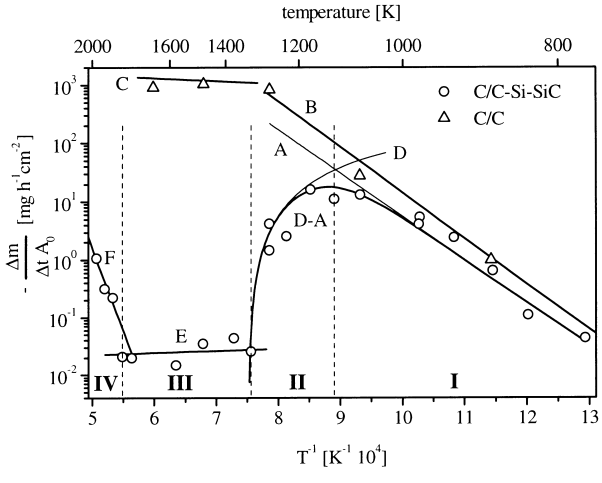

Fig. 10. Temperature dependence of the oxidation rates for silicon/silicon carbide coated C/C material and uncoated C/C material (solid curves: see text, vertical dashed lines: limits of the temperature ranges, horizontal dashed line: maximum mass loss rate for long-term applications).

II. The oxidation rate drops with increasing temperature ($1123 < T < 1323$ K). The overall reaction is determined by the gas diffusion in the cracks. With increasing temperature the cracks close and the fractional area of the cracks f_R decreases. The temperature dependence of the gas interdiffusion influences the kinetics slightly. The calculation of the reaction rate was performed by neglecting Knudsen diffusion ($\bar{D} = D_G$) since the critical crack width of about 10 nm is reached only for $T_c - T = 5$ K. Furthermore the formation of SiO_2 is ignored because of the very low (parabolic) rate constant in this temperature range. The solution of the differential eqn (18) for an oxygen concentration at the surface $n(d_L) = n_0$ ($\sim 2 \cdot 10^4$ Pa) and for a constant convectional flow velocity:

$$j_{o_2} = D_{G_{d_L}}^{n_G} \ln\left(\frac{n_0}{n_G} + 1\right) \tag{24}$$

Here, n_G is the total gas density ($\sim 10^5$ Pa). The curve D in Fig. 10 results from calculation with a distribution of the crack width in the range from $d_{W0} = 1{\cdot}2\ \mu$m to $d_{W1} = 2{\cdot}2\ \mu$m. The agreement between experiment and calculation around 1123 K is improved by considering a mixed control (steps 2 and 5) as curve D–A in Fig. 10 shows. Under these assumptions the oxygen partial pressure drop in the cracks is nearly linear (curve P in Fig. 12). The resulting average crack width $\bar{d}_W = 1{\cdot}65\ \mu$m at room temperature [see eqn (2)] is slightly lower than the crack width measured by optical microscopy $\bar{d}_W \sim 2\ \mu$m. This is likely due to the fact that a fraction of the cracks follow a tortuous path within the coating thereby decreasing the effective crack width.

III. Temperature independent regime ($1323 < T < 1823$ K). The oxidation rate exhibits only a weak temperature dependence which indicates a control by gas phase diffusion. Assuming open cracks of $d_W = 7{\cdot}6$ nm curve E in Fig. 10 results ($\bar{D} = D_K$) from eqn (24). Under these conditions the velocity of the convectional outward gas flow is $v = 1$ cm s^{-1}. The corresponding calculation for nearly totally closed cracks (99% of the length) led to diffusion channels with an effective width of $d_W = 15$ nm ($\bar{D} = D_G$). These crack widths are very small and they must be closed in short periods of time if the formation of

SiO_2 is to be undisturbed. For $p_{o2} = 2 \cdot 10^4$ Pa and 1473 K SiO_2 layers of 7 nm were formed on CVD–SiC within 100 s (estimation by using data from[11]). In the following attention is focussed on the problem: Why do cracks remain open? In order to obtain information about the formation of SiO_2 the oxygen partial pressure inside the cracks is calculated. Initially, wedge-shape cracks as shown in Fig. 11 were considered. SiO_2 is formed preferentially in the upper crack region until a steady state or a very slow oxidation kinetics is reached. The crack width is d_W and εd_W at the surface and at the bottom, respectively (assumption: $\varepsilon = 20$). Because the velocity v, the oxygen flux density j_{o2} and the (Knudsen) diffusion coefficient all depend upon the position in the crack, the solution of eqn (18) is more complicated. It can be performed by means of the transformation

$$\tilde{x} = x + d_L\left(\frac{\varepsilon}{\varepsilon - 1} - 1\right) \tag{25}$$

which results in:

$$d_W \sim \tilde{x}, \bar{D} = D_K \sim \tilde{x}, \quad j \sim \frac{1}{\tilde{x}}, v \sim \frac{1}{\tilde{x}} \tag{26}$$

Then, the solution of eqn (18) yields:

$$n(\tilde{x}) = n_{tot}\left(e^{a j_1\left(\frac{1}{x} - \frac{1}{\tilde{x}_2}\right)} - 1\right) \tag{27}$$

With:

$$a = \sqrt{\frac{\pi M}{8RT}}\frac{3\tilde{x}_1^2}{D_0 d_W n_G}, \tilde{x}_1 = d_L\left(\frac{\varepsilon}{\varepsilon - 1} - 1\right), \tag{28}$$

$$\tilde{x}_2 = d_L\frac{\varepsilon}{\varepsilon - 1}$$

Here j_1 is the oxygen flux density at the surface. For $d_W = 1 \cdot 7$ nm curve E is obtained in Fig. 10. The resulting large oxygen partial pressure drop (curve K1 in Fig. 12) is non-linear. Because of the considerable outward gas flow ($v = 4 \cdot 6$ cm s^{-1}), the nominally stagnant atmosphere in the furnace and the SiO_2 layer on the surface of the sample (Fig. 11) the oxygen partial pressure must be lower than $2 \cdot 10^4$ Pa at $= d_L$. Assuming $p_{o2}(d_L) = 2 \cdot 10^3$ Pa curve K2 in Fig. 12 results.

The next key issue in connection with the open question is the calculation of the transition oxygen pressure for the active-to-passive oxidation transition. Wagner's theory predicts a transition pressure p_{o2}^{T1} corresponding to:

$$p_{o2}^{T1} = \frac{D_{SiO}}{D_{o_2}}\frac{\delta_{o_2}}{\delta_{SiO}}p_{SiO}^{eq}, \delta_i = \sqrt{D_i t}, i = O_2, SiO \tag{29}$$

With equilibrium pressures taken from[12] curve p_{o2}^{T1} in Fig. 13 is obtained which agrees with experimental results ([13], curve p_{o2}^{TN} in Fig. 13). However, the experimental conditions used in this investigation were different: Because of the outward gas flow δ_{o2} is increased and δ_{SiO} is decreased. Assuming $\delta_{o_2}/\delta_{SiO} = 10$ (curve p_{o2}^{T2} in Fig. 13) the existence of a transition oxygen pressure of $2 \cdot 10^3$ Pa at approximately 1673 K seems to be possible. The calculation allows the following conclusion: The outward gas flow yields an oxygen partial pressure which stops or decelerates considerably the formation of SiO_2 in the cracks. Note that in the temperature range HI there is a constant mass loss rate which indicates that active oxidation does not occur.

IV. The oxidation rate increases with temperature (1823 K < T). Because of the limited number of data points the appearance of an exponential temperature dependence of the reaction rate is not sure. Furthermore, the samples reacted with the sample support at 1973 K (eutectic temperature in the system SiO_2–Al_2O_3: 1860 K[14]).

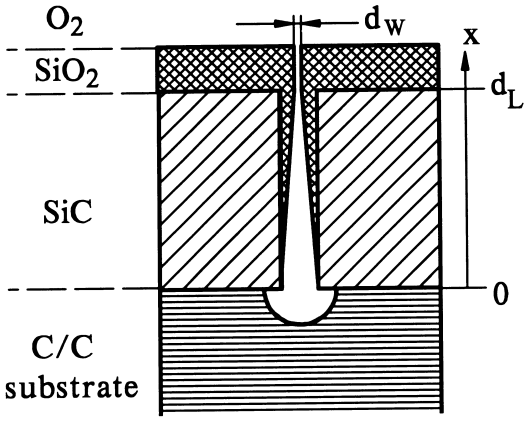

Fig. 11. Model: Scheme of the wedge-shape cracks.

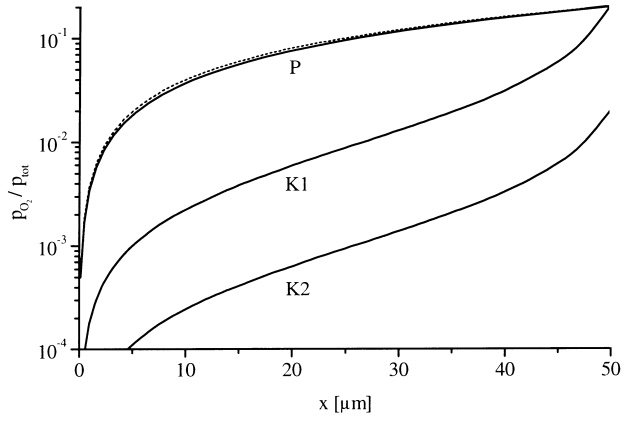

Fig. 12. Oxygen partial pressure in the cracks (see text).

Apparently, in the temperature range above 1823 K the oxygen pressure for the passive-to-active transition reaches values which are higher than the oxygen pressure in the cracks. Consequently, the crack walls are consumed. The calculation (exponential temperature dependence) yields curve F in Fig. 10.

4.5 Summary of the oxidation mechanisms of the reference material

- Silicon carbide coatings are effective only beyond 1323 K. Because of the thermal expansion coefficient mismatch between substrate and coating system cracks exist below this temperature which lead to a high oxygen permeation through the coating. Model calculations confirm the predominant role of cracks.
- In the temperature range from 1323 to 1823 K the oxidation rate is close to the limit for long term applications. Furthermore a mass loss is observed which corresponds to fibre degradation.
- Beyond 1823 K the reference material is destroyed rapidly. The active oxidation behaviour of SiC determines the oxidation rate.

5 Oxidation Behaviour of the Mullite Coated Material (C/C–Si–SiC–SiO_2–mullite)

5.1 Isothermal oxidation in air

Thin mullite layers (~900 nm) on C/C–Si–SiC substrates did not improve the oxidation resistance. Beyond 1823 K the oxidation rates were close to the oxidation rates of the reference material. In the range $1473 \leq T \leq 1723$ K samples with both mass loss and mass increase were observed. This means that the reliability of the layers is not satisfactory. Apparently, pores and microcracks were not closed by thin mullite coatings.

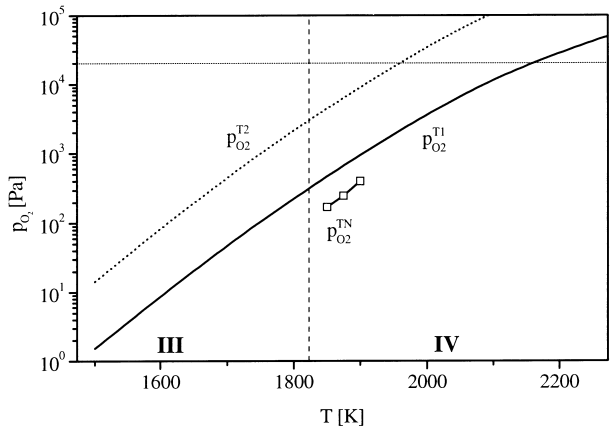

Fig. 13. Transition oxygen partial pressures (see text).

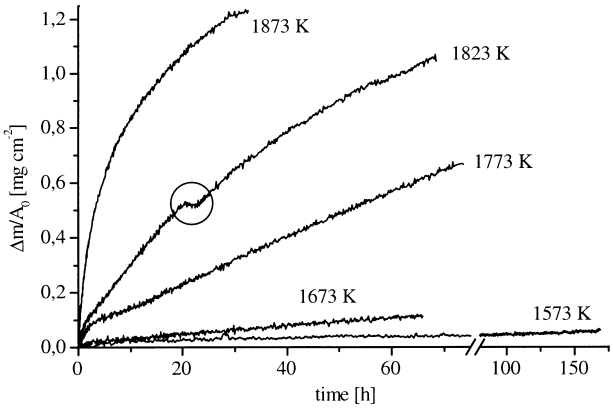

Fig. 14. Specific mass change of preoxidized and mullite coated C/C–Si–SiC material (mullite layer thickness 2·5 μm) as a function of time.

The improved sample preparation as described in section 2 (preoxidation of the substrate, mullite layer thickness: 2·5 μm), led to a mass gains (Fig. 14) as discussed in section 5·4. As can be seen from the marked region in Fig. 14 mullite can seal defects at temperatures close to the eutectic temperature (1860 K[14]).

Figure 15 shows cross sections of representative samples after the TGA experiments. The observed thicknesses agree with calculated values from the mass gain. At elevated temperatures a glassy layer appears which levels out the roughness of the surface.

5.2 Phase analysis by IR spectroscopy

After TGA at elevated temperatures in air the reflection spectra show the formation of amorphous SiO_2, which is indicated by its peak structure with a maximum at 1100 cm^{-1} and a shoulder at 1200 cm^{-1} which is typically obtained for SiO_2 glasses (Fig. 16). Thermogravimetric data show a mass gain throughout the temperature range pointing to the formation of SiO_2. The amount of SiO_2 formed, calculated using the thermogravimetric measurements, can be expressed in terms of the equivalent thickness of a SiO_2 layer. Values of about 1·5, 9·1, and 16·6 μm are obtained for the samples heated at 1673, 1773, and 1873 K, respectively.

At 1673 K SiO_2 is not observable at the surface by means of IR reflectance spectroscopy. Consequently, SiO_2 must be formed at the inner SiC–mullite interface. At higher temperatures the interdiffusion at the SiO_2–mullite interface becomes important.

However, the existence of mullite for samples annealed at 1773 and 1873 K is difficult to ascertain from the IR reflection spectra, due to the strong increase of the SiO_2 content.

5.3 ^{18}O diffusion

Simultaneously, measurements of oxygen diffusion (^{18}O) in the mullite layers were performed. Here,

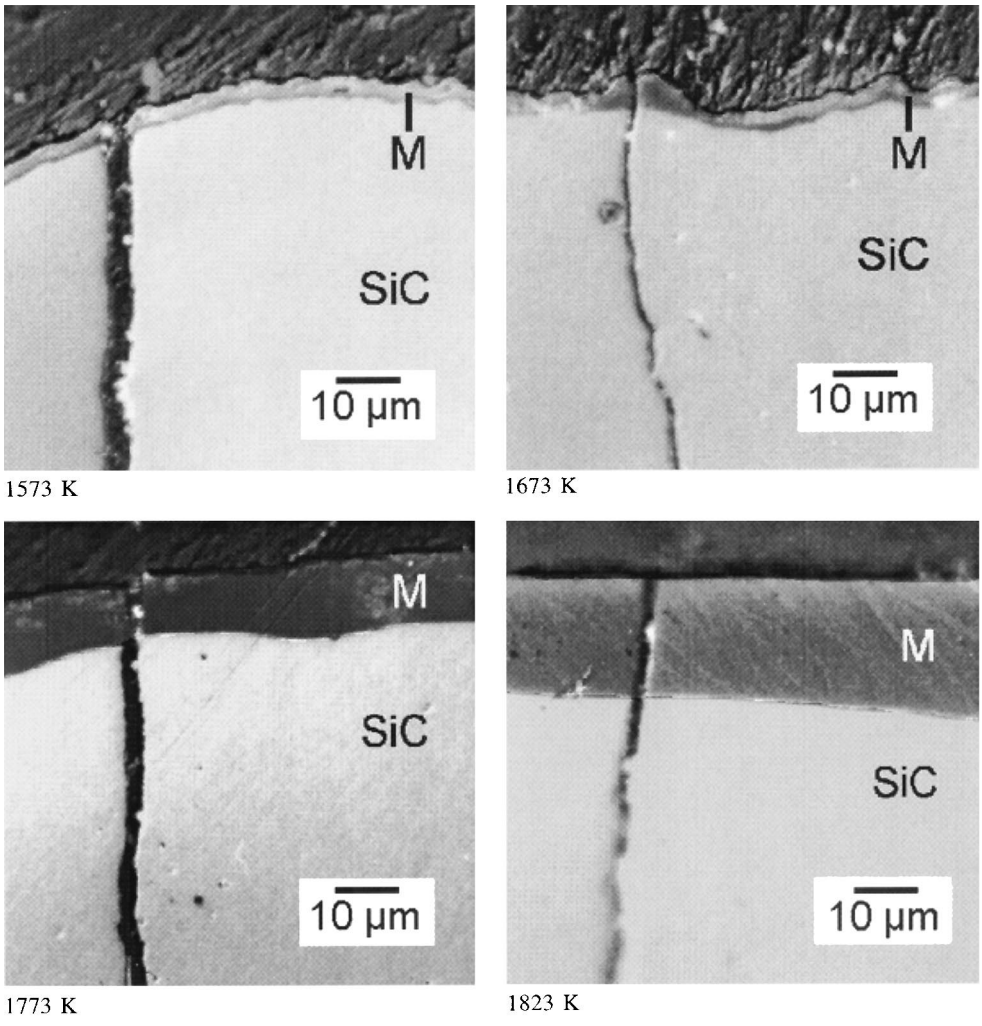

Fig. 15. Cross sections of mullite (M) coated C/C–Si–SiC samples after the TGA experiments (outermost regions only).

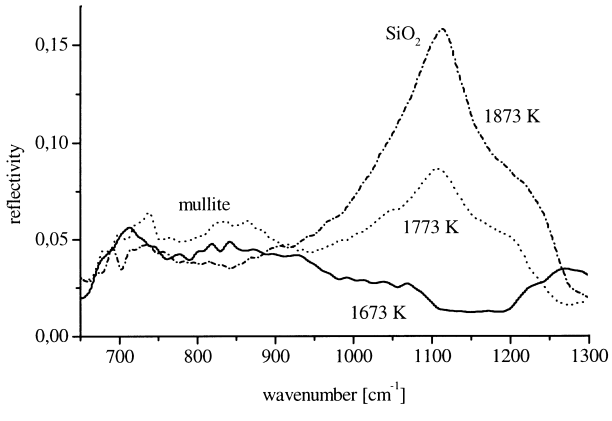

Fig. 16. Comparison of reflectivity spectra of PLD coatings on C/C–Si–SiC substrates annealed at different temperatures in air.

the coatings were deposited on SiC* slabs so as to exclude effects caused by the reaction of ^{18}O with the C/C matrix. In order to investigate the influence of preoxidation in ambient air three types of preparation were used:

A. Without preoxidation.

B Preoxidation: conditions corresponding to oxidation in $^{18}O_2$ (see parameters in Table 2).

C. Preoxidation: 1823 K, 1 h.

It should be noted that preoxidation type C led to pronounced formation of SiO_2. The layer thickness increased to about 20 μm (original thickness: 2·5 μm). Thus, the content of Al_2O_3 dropped dramatically.

After pretreatment, all samples were oxidized in 98% $^{18}O_2$ (2% $^{16}O_2$) at a total pressure of 2·10 Pa. For all ^{18}O oxidations the same set of parameters were used (Table 2).

All samples were analyzed using a secondary neutral mass spectrometer† (SNMS). Because of additional comparison between WDX measurements and the SNMS data it could be conducted that the sensitivity factor for aluminium is not matrix independent as suggested in the literature.[15] On the contrary, the sensitivity factor for oxygen is constant and the SNMS signal can be interpreted as a concentration. For representative samples a determination was made of the ratio of the sputter rate in the protective layer and in the substrate material in order to perform the depth scale calibration.

As a satisfactory approximation for short diffusion times a fit of the solution of Fick's second law

*Produced by BCE Special Ceramics GmbH, Germany.
†Simslab, VG Scientific, Great Britain.

for a constant surface concentration [eqn (30)[16]] was made to the data generated in this investigation in order to obtain the oxygen tracer diffusivity (D) values given in Fig. 17.

$$n(x) = (n_0 - n_s)\mathrm{erf}\left(\frac{\mathrm{x}}{2\sqrt{D\mathrm{t}}}\right) + \mathrm{n}_s \qquad (30)$$

n = concentration,
n_0 = concentration in the bulk,
n_s = concentration at the surface.

Thereafter, a calculation was made of the diffusion parameters D_0 and E_A by fitting eqn (31) to the diffusion coefficients (Table 3).

The diffusion parameters resulting from preoxidation type C are comparable to representative diffusion data of oxygen in SiO_2.[17] As mentioned above this layer contains only a small amount of Al_2O_3.

$$D = D_0 \mathrm{e}^{-\frac{E_A}{\mathrm{RT}}} \qquad (31)$$

D_0 = preexponential factor,
E_A = activation energy

Table 2. Parameters of preoxidation and ^{18}O treatment

Type of preoxidation	*Preoxidation* T *[K]/t [min]*	*^{18}O treatment* T *[K]/t [min]*
A	Without preoxidation	
	1473/120	1473/240
B	1573/40	1573/80
	1673/15	1673/30
	1773/5	1773/10
C	1823/60	

The diffusion coefficients after the preoxidations A and B do not show differences. Therefore it can be concluded that there are no open pores in the deposited mullite layer. Furthermore the diffusion coefficients of oxygen in mullite are one or two orders of magnitude lower than in SiO_2 glass.

5.4 Analysis of the reaction kinetics

The oxidation behaviour of the samples coated with a 'thick' mullite film (improved sample preparation, see above) shows different kinetics depending on the temperature range (Fig. 14). Because of SiO_2 formation all samples exhibit a mass increase.

A comparison is made of the oxidation behaviour with the passive oxidation of uncoated Si or SiC which is parabolic. Because of the deposited mullite layer the parabolic behaviour is only visible if the thickness of the SiO_2 layer formed during the oxidation experiments is not negligible with respect to the mullite layer. As long as only a thin layer of SiO_2 is formed at the inner interface the oxidation behaviour apparently remains linear.

A simple model with the following assumptions is proposed (Fig. 18):

1. The kinetics of the reaction is controlled by the diffusion of oxygen across the mullite layer and the SiO_2 layer. The rate of the reaction (13) is sufficiently high in order to assume that the concentration of free oxygen at the inner interface n_0 is zero.
2. The concentration of mobile oxygen atoms at the surface n_s is the fit parameter. It should be a small fraction of the total oxygen concentration in stoichiometric mullite.

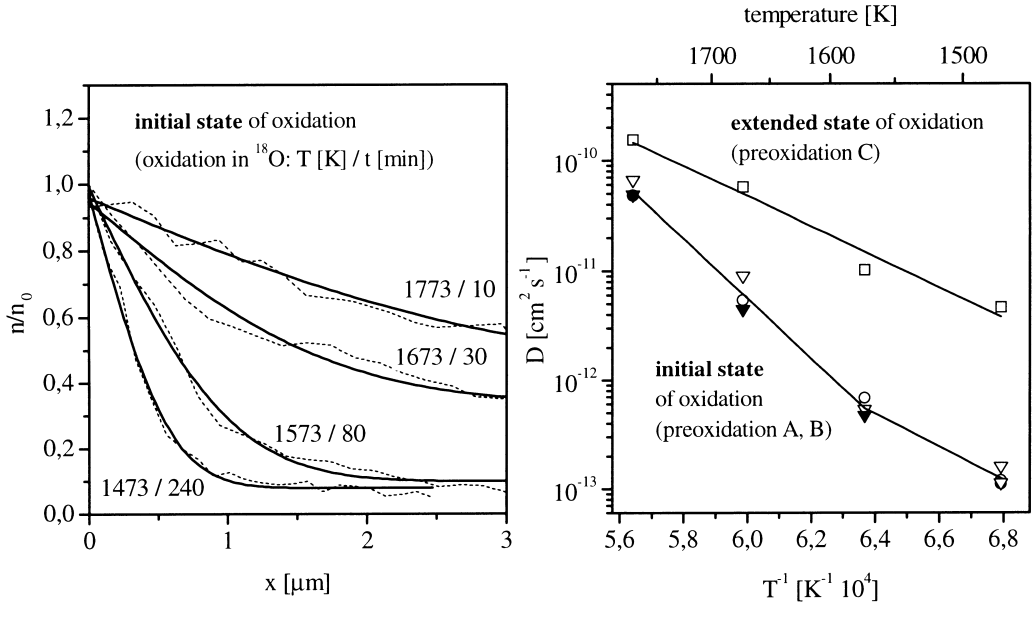

Fig. 17. Depth profile of ^{18}O in PLD mullite after different oxidation and preoxidation treatments (left), corresponding diffusion coefficients of ^{18}O in PLD mullite (right).

3. There is no interdiffusion of the metal ions at the inner interface.

Thus the flux of oxygen atoms across the mullite layer is equal to:

$$j(t) = -D_M \frac{n_1(t) - n_s}{x_M} \tag{32}$$

The corresponding flux in SiO_2 is:

$$j(t) = -D_s \frac{n_0 - n_1(t)}{x_S(t)} \tag{33}$$

j = flux of oxygen atoms,
D_M, D_S = oxygen diffusion coefficients in mullite and in amorphous SiO_2, respectively,
n_s, n_1, n_0 = concentrations of mobile oxygen,
x_M, X_S = thicknesses of the mullite layer and of the SiO_2 layer, respectively

The increase of the thickness of the SiO_2 layer can be described by:

$$\frac{dx_s}{\mathrm{dt}} = \frac{1}{3} v j(t) \tag{34}$$

v = volume of a SiO_2 molecule.

The factor 1/3 takes into account the formation of one SiO_2 molecule (together with one CO molecule) from three oxygen atoms according to reaction (13).

Table 3. Diffusion parameters in PLD mullite

Type of preoxidation	*Temperature range [K]*	D_0 [$cm^{-2} s^{-1}$]	E_A [$kJ mol^{-1}$]
A, B	1473–1573	$2{\cdot}2{\cdot}10^3$	289
	1573–1773	$2{\cdot}2{\cdot}10^5$	530
C	1473–1773	336	264

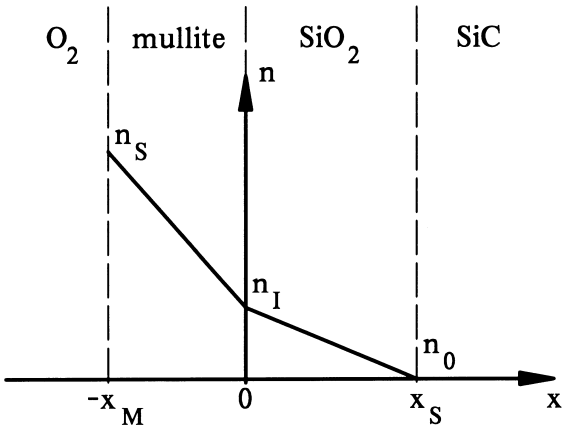

Fig. 18. Scheme of the oxygen concentration in the layer system mullite–SiO_2–SiC.

The increase of the SiO_2 layer thickness (which is proportional to the mass gain) is calculated by eliminating $n_1(t)$ in eqns (32) and (33). The resulting expression is inserted into eqn (34) which yields upon integration:

$$x_S(t) = \alpha\left(\sqrt{1 + \beta t} - 1\right) \tag{35}$$

With:

$$\alpha = \frac{D_S}{D_M} x_M, \beta = \frac{2}{3} v n_s \frac{D_M^2}{D_S} \frac{1}{x_M^2} \tag{36}$$

For the oxidation kinetics the transition from linear to parabolic behaviour is of particular interest.

For $\beta t \ll 1$ eqn (35) yields linear kinetics:

$$x_S(t) = \frac{1}{3} v n_s \frac{D_M}{x_M} t \tag{37}$$

Whereas $\beta t \gg 1$ leads to parabolic kinetics:

$$x_S(t) = \sqrt{\frac{2}{3} v n_S D_S} \sqrt{t} \tag{38}$$

The transition time t_T is defined by:

$$\beta t_T = 1 \tag{39}$$

The transitions times t_T (Table 4) are calculated using the measured diffusion coefficients (Table 3). In the case of T = 1873 K the diffusion coefficients are extrapolated according to eqn (31).

In agreement with the experiments this simple model shows that after long times the oxidation kinetics become parabolic. The transition time decreases with increasing temperature. To compare the TGA experiments for short times and long times to the calculations the oxidation rates were determined from eqn (35) and subsequently the conversion to a mass change was given by:

$$\left(\frac{1}{A_0}\frac{\mathrm{dm}}{\mathrm{dt}}\right)_t = \frac{\rho_{SiO_2}}{6} \frac{\alpha\beta}{\sqrt{1 + \beta t}} \tag{40}$$

The calculated oxidation rates resulting from the diffusion parameters of preoxidation type A (= B) and C are shown in the Arrhenius plot (Fig. 19). The fit parameter n_s results in a concentration of

Table 4. Calculated transition times t_T

Temperature [K]	*1473*	*1573*	*1673*	*1773*	*1873*
t_T [h]	$8{\cdot}2\ 10^4$	$1{\cdot}7\ 10^4$	443	18	1

the mobile oxygen atoms of 3% of the total oxygen concentration in stoichiometric mullite: $n_s = 0{\cdot}03{\cdot}13{\cdot}\rho/M_{mullite} = 1{\cdot}7{\cdot}10^{21}$ cm^{-3}.

5.5 Layer composition after the oxidation treatments

Confirmation of the disappearance of mullite after extended oxidation treatments at elevated temperatures requires investigation of the layer composition. WDX analyses of cross sections of a sample heated for 70 h at 1823 K (Fig. 20) show a relatively slow fall in aluminium concentration within the scale. The aluminium content is much lower than in the as-deposited layer. Obviously, mullite is dissolved in the newly formed SiO_2.

In order to estimate the effective aluminium diffusivity, the (independent) interdiffusion of silicon and aluminium between the mullite layer and the growing SiO_2 layer, is taken into account. Choosing $D_{Al} = 10^{-11}$ cm^2 s^{-1} the A1 curve in Fig. 20 results. The oxygen diffusivity is taken from the SNMS measurements. The calculated mass gain [see eqn (40)] agrees very well with the TGA experiments.

5.6 Oxidation under thermal cycling

The mullite coated material was also tested under thermal cycling conditions. Step motors allowed the furnace to be moved so as to give a nominal cooling/heating rate of ∓ 20 K s^{-1}.

Because of the very small difference in thermal expansion coefficients of SiC and mullite spallation of the mullite layer was not expected.

The thermogravimetric data for cycling between room temperature (10 min) and 1673 K (2 h) are shown in Fig. 21. During the high temperature steps the mass gain is comparable to the isothermal oxidation behaviour (see insert in Fig. 21). Cooling

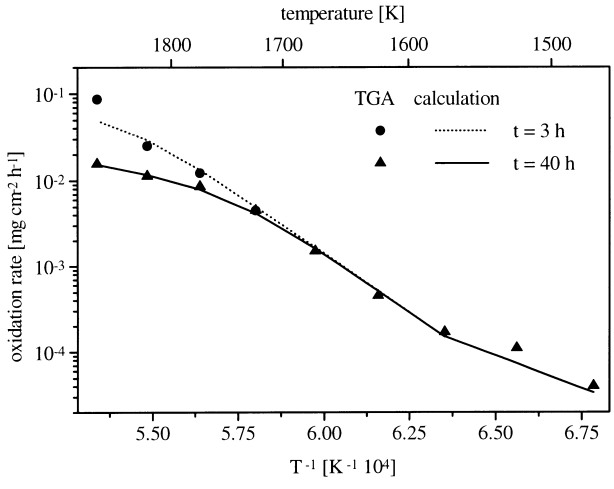

Fig. 19. Calculated and measured temperature dependence of the oxidation rate for preoxidized and mullite coated C/C–Si–SiC material.

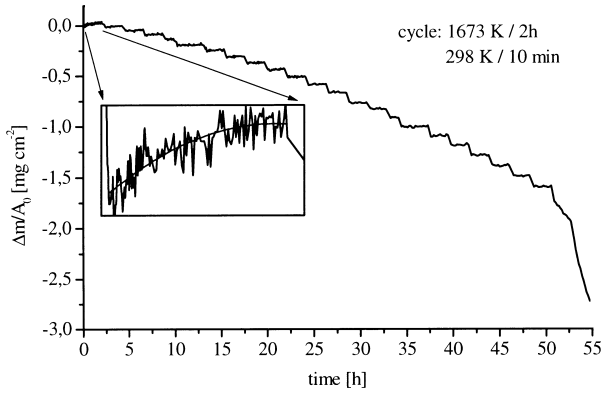

Fig. 21. Specific mass change of preoxidized and mullite coated C/C–Si–SiC material (mullite layer thickness 2·5 μm) under thermal cycling between room temperature and 1673 K.

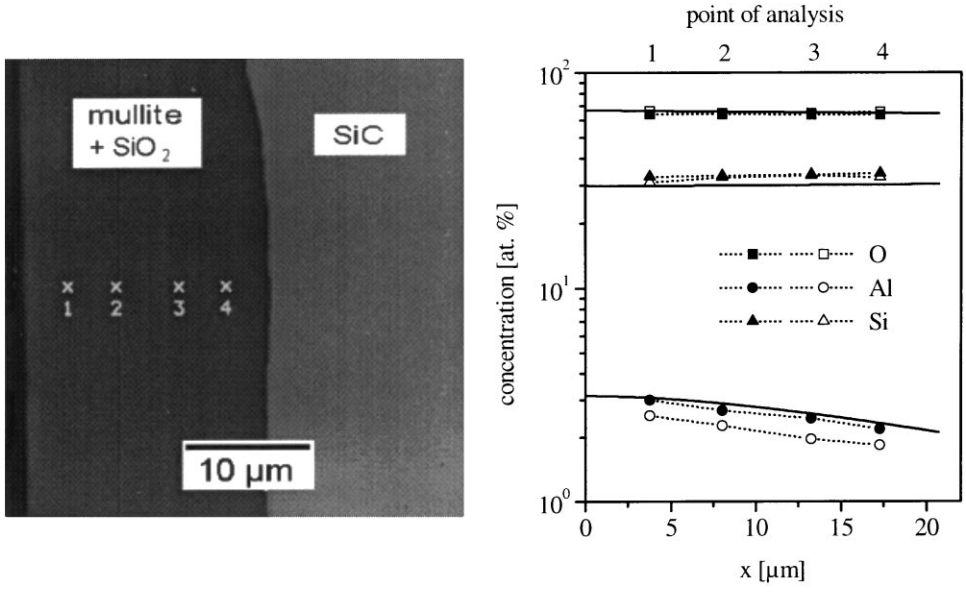

Fig. 20. Cross-section (SEM) of mullite coated C/C–Si–SiC oxidized at 1823 K for 90 h and the corresponding concentrations measured (symbols and dashed lines) by WDX and calculated (solid lines).

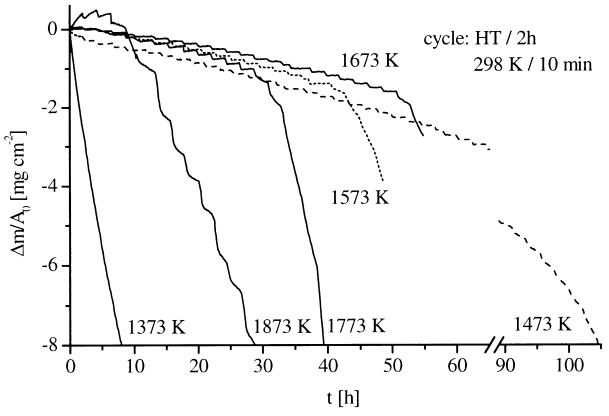

Fig. 22. Specific mass change of preoxidized and mullite coated C/C–Si–SiC material (mullite layer thickness 2·5 μm) under thermal cycling between room temperature and 1373–1873 K.

down to room temperature leads to opening of the cracks in the SiC layer as the thin mullite layer is not able to close cracks with an average width of 2 μm at room temperature. The mean mass loss during one cooling and heating cycle ($\Delta m_{cycle}/A_0$) was 0·08 mg cm^{-2} which corresponds to the result of the calculation via eqn (41):

$$\frac{\Delta m_{cycle}}{A_0} = 2 \int_{T_R}^{T_H} \frac{k_L(T)}{\nu} dT \qquad (41)$$

Below 1323 K the mullite layers are not protective and so the oxidation rate $k_L(T)$ of the reference material [eqn (6)] can be used. ν is the rate of temperature change (20 K s^{-1}), T_H and T_R are the temperature limits of 1673 and 293 K, respectively.

Figure 22 shows the mass change during thermal cycling between room temperature and 1373–1873 K. The best cyclic oxidation resistance was observed at 1473 K. Above this temperature the crack width increased during cycling.[18] At 1373 K the cracks were not sealed.

It was observed that after oxidation under thermal cycling conditions spallation of the SiC layer of the substrate material occured. The latter is responsible for the breakdown of the oxidation resistance.

6 Conclusion

Mullite coatings with a thickness of 2·5 μm and a preoxidation treatment of the C/C–Si–SiC substrate material improved the oxidation behaviour of CVD–SiC coated C/C composites. As expected, all samples exhibit a mass gain. In the temperature range $1473 \leq T \leq 1873$ K the inward diffusion of oxygen across the outer mullite containing layer controlled the kinetics of the reaction, as was deduced from ^{18}O diffusivity measurements in pulsed laser deposited mullite layers.

Under thermal cycling conditions the cracks in the SiC layer of the substrate material and the spallation of this layer were responsible for the final breakdown of the oxidation resistance.

Acknowledgements

The help of E. Ebeling with the preliminary oxidation runs was most valuable. M. Göbel kindly helped with the ^{18}O treatment. Financial support of the Deutsche Forschungsgemeinschaft made this work possible.

References

1. Luthra, K. L., Singh, R. N. and Brun, M. K., Toughened silcomp composites—process and preliminary properties. *J. Am. Ceram. Soc.*, 1993, **72**, 79.
2. De Castro, L. D. and McEnaney, B., The control of high temperature corrosion of engineering carbons and graphites. *Corros. Sci.*, 1992, **33**, 527.
3. Danes, F., Saint-Aman, E. and Coudrier, L., The Si–C–O system. *J. Mat. Sci.*, 1993, **28**, 489.
4. Luthra, K. L., Oxidation of carbon/carbon composites—a theoretical analysis. *Carbon*, 1988, **26**, 217.
5. Jacobson, N. S., Corrosion of silicon–based ceramics in combustion environments. *J. Am. Ceram. Soc.*, 1993, **76**, 3.
6. Lee, K. N., Miller, R. A. and Jacobson, N. S., New generation of plasma-sprayed mullite coatings on silicon carbide. *J. Am. Ceram. Soc.*, 1995, **78**, 705.
7. Schultrich, B., Lenk, A., Witke, Th., Borchardt, G. and Fritze, H., Pulsed laser deposition of oxide films by multi-kilowatt CO_2 lasers. *J. Appl. Surf. Sci.*, 1997, **109–110**, 362–365.
8. Ocana, M., Fornes, V., Garcia-Ramos, J. V. and Serena, C. J., Polarization effects in the infrared spectra of α-quartz und α-cristobalite. *Phys. Chem. Minerals*, 1987, **14**, 527.
9. Strife, J. R. and Sheehan, J. E., Ceramic coatings for carbon-carbon composites. *Ceram. Bul.*, 1988, **67**, 369.
10. Geiger, G. H. and Poirier, D. R., *Transport Phenomena in Metallurgy*, Addison-Wesley Publishing Company 1973, pp. 463.
11. Ogbuji, U. J. T. and Opila, E. J., A comparison of the oxidation kinetics of SiC and Si_3N_4. *J. Electrochem. Soc.*, 1995, **142**, 925.
12. Heuer, A. H. and Lou, V. L. K., Volatility diagrams for silica, silicon nitride, and silicon carbide and their application to high-temperature decomposition and oxidation. *J. Am. Ceram. Soc.*, 1990, **73**, 2789.
13. Narushirna, T., Goto, T., Iguchi, Y. and Hirai, T., High-temperature active oxidation of chemically vapor deposited silicon carbide in an Ar-O_2 atmosphere. *J. Am. Ceram. Soc.*, 1991, **74**, 2583.
14. Aramaki, S. and Roy, R., Revised phase diagram for the system Al_2O_3–SiO_2. *J. Am. Ceram. Soc.*, 1962, **45**, 229.
15. Wucher, A. and Oechsner, H., Depth scale calibration during sputter removal of multilayer systems by SNMS. *Fresenius'Z. Anal. Chem.*, 1989, **333**, 470.
16. Philibert, J., *Atom Movements; Diffusion and Mass Transportin Solids*, Les éditions de physique, 1991, p. 7.

17. Kahlen, J. D., Boyce, R. S. and Cawley, J. D., Oxygen tracer diffusion in vitreous silica. *J. Am. Ceram. Soc.*, 1991, **74**, 203.

18. Lamouroux, F., Camus, G. and Thebault, J., Kinetics and mechanisms of oxidation of 2D woven C/SiC composites: I, experimental approach. *J. Am. Ceram. Soc.*, 1994, **77**, 2049 .